

Strain Measurement with Fiber Bragg Grating Sensors

by Manfred Kreuzer

HBM, Darmstadt, Germany

Fiber Bragg Grating Sensors (FBGS) are gaining increasing attention in the field of experimental stress analysis. They are very well suited to the new materials of glass and carbon fiber reinforced composites which are often used for highly stressed constructions, e.g. in airplanes and wind power plants. Basically, Fiber Optic Bragg Sensors are strain-measuring devices and therefore provide many of the advantages of the well known metal foil strain gages. This paper gives a short introduction to FBG sensors, points out their special strengths and weaknesses and describes a measuring system which enables strain gages and FBGS to be measured simultaneously, providing all data processing functions originally developed for the strain gages also for the FBGS signals, like signal conditioning, rosette calculations, filtering, Fourier transformation, free definable mathematics etc. Such systems are especially useful in tests where both strain gages and FBGS are used.

1. Short History of Optical Fibers

The history of optical fibers reaches back to the 1960ties. In 1969, first gradient index fibers were manufactured by the cooperation of Nippon Sheet Glass Co. and Nippon Electric Co. for telecommunication applications. But these fibers still had a damping of 100 dB/km caused mainly by chemical impurity of the glass. Great progress was made in the following years and in 1976 improved fibers with <1dB/km were available in Japan, USA and Great Britain. Infrared was used then instead of visible light. Today the damping is <0.2 dB/km. The best suited glass for fibers is fused silica (SiO_2) [1].

In 1978, Ken O. Hill found the effect of photo sensitivity for Germanium doped fibers. Exposure to ultraviolet light induces a permanent change of the refractive index. The next step was to use this effect and write Bragg gratings into fibers which then can reflect very small wavelength peaks. The wavelengths of these peaks change with temperature or when such fibers are strained. First commercial Fiber Bragg Grating Sensors were available in 1995 from 3M and Photonics. Since 2000 more than 20 companies offer Fiber Bragg Gratings.

2. Features of Fiber Bragg Gratings

Because FBG sensors can measure strain (and not displacement) they also provide the superior advantages of the strain measuring principle, as metal foil strain gages do. Like strain gages, FBG can be used to build transducers for measuring many different physical quantities. But this is not the subject of this paper. In the following only the characteristics of the FBG will be explained.

Though FBG cannot fully compete with metal strain gages regarding price and precision, they provide some superior qualities making them very suited to special applications:

- FBG match quite well with new composite materials like glass or carbon fiber reinforced composites which are widely used in modern constructions, like new airplanes or in wind power plants. FBG can directly be integrated into composites or can be fixed directly or as patches on the surface of the test object like normal strain gages.
- FBG can measure very high strain (>10,000 $\mu\text{m}/\text{m}$) and are therefore very well suited to highly stressed composite constructions.

- FBG are small sized and lightweight
- FBG are immune to electromagnetic interference (even lightning interference)
- FBG are intrinsically passive (no electrical power necessary); and therefore can be positioned in high voltage and potentially explosive atmosphere areas
- FBG signals are not distance-dependent (up to >50 km connection length is possible)
- On a single fiber many Fiber Bragg Gratings can be located in a row (>20 FBG; with special interrogator technologies up to >100). No return fiber is needed (but often preferred because of redundancy reasons)
- Long term stability is very high
- Good corrosion resistance
- Special versions of FBGS can be used at very high temperatures (>700 °C)
- FBG are also advantageously used in cryogenic environment because of their low thermal conductivity of the single fiber feeding many sensors and their stable optical properties with very low residual temperature dependencies near to liquid helium temperatures.
- Very low magnetic field interactions
- Ease of installation (time, cabling, testing)

Of course there are also some properties that have to be mentioned where FBGS show some weaknesses:

- FBG show high temperature dependence ($\Delta\lambda/\lambda_0$ caused by 1°C is equivalent to $\Delta\lambda/\lambda_0$ caused by 8 $\mu\text{m}/\text{m}$ mechanical strain). Temperature compensated FBGS are not yet available. Temperature compensation requires special arrangements and read-out of two FBG
- FBG cannot provide self-compensation of apparent strain (thermal expansion coefficient α of steel, aluminum or fiber composites). Temperature compensation has to be done by separate temperature-measuring channels and corresponding calculations.
- FBG show high sensitivity to lateral forces or pressure causing light birefringence. The refraction coefficient becomes different for the 0° and 90° axis of polarized light, resulting in two separate reflection peaks. However, depolarized light and optical peak shaping in the polychromator based FBG sensor system (Chpt. 7, Fig.11) can solve this problem.

- Gage factor is only $k = 0.78$ (0.77 ...0.81) and can be different from fiber type to fiber type.
- The small size of strain gages cannot be reached with FBG patches
- The stiffness of FBG sensors is higher than that of foil strain gages causing higher parallel force to the specimen.
- The sensing fiber core is positioned at a greater distance from the specimen surface. This can cause calibration errors when the patch is applied on curved surfaces.
- The radius of the fiber should be >10 mm; FBG rosettes therefore tend to be quite large
- Interrogator instruments for FBG sensors are still expensive (however with many sensors per interrogator the channel cost including installations can be lower than foil strain gages).

3. Fiber Bragg Grating Sensors (FBGS)

Bragg gratings are written into so called single-mode fibers. These fibers consist of a very small inner core of 4 to 9 μm diameter and an outer part (cladding) of pure glass (SiO_2) of 125 μm diameter. The core has a higher refractive index caused by high Germanium doping. The difference of refraction indexes between inner core and cladding causes the light to propagate only inside the small core. The glass fiber is coated with acrylate, polyimide or ORMOCER (organic modulated ceramic) to protect it especially against water and hydrogen which causes crack growing and can reduce the mechanical stability (the breaking point may decrease from $>30,000$ $\mu\text{m}/\text{m}$ to only 5,000 ...1,000 $\mu\text{m}/\text{m}$). To write the Bragg grating into the fiber core the fiber must first be dismantled of the coating and afterwards newly coated. This process has to be done very thoroughly, otherwise the mechanical stability of the fiber may suffer severely and the fiber may break already at low strain levels.

To measure strain the sensors must be fixed to the specimen, typically by gluing.

Stretching a strain gage sensor causes a change in resistance of the metal grid (Fig. 1).

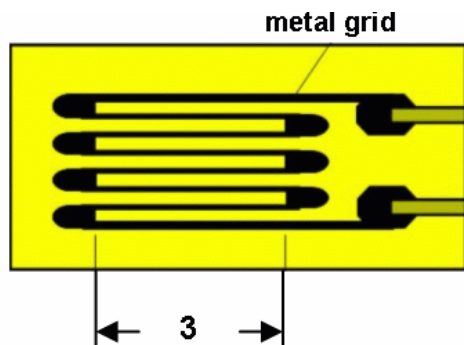


Fig 1: Strain gage schematic

Stretching a Fiber Optic Bragg sensor causes a change in grating period (Fig. 2) resulting in a change in wavelength of the reflected ultraviolet light.

Bragg gratings reflect wavelengths which have very small bandwidths (so-called peaks in the spectrum).

The grating consists not only of some fringes as shown in Fig. 2 but of several thousand fringes.

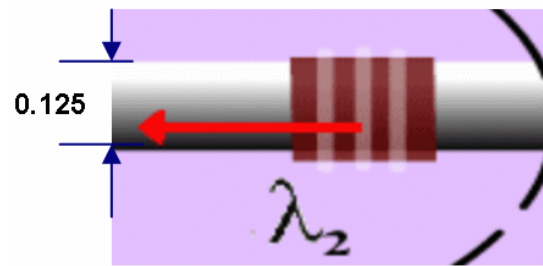


Fig. 2: Fiber Bragg Grating schematic

Each single fringe reflects a very small part of all incoming wavelength. The reflection factor per single fringe is in the range of only 0.001% ...0.1% depending on how much energy was used to write the Bragg grating and on the percentage of Germanium doping of the fiber core.

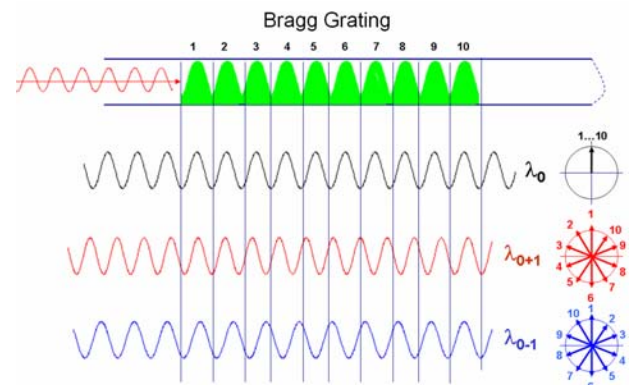


Fig. 3: Functional principle of Fiber Bragg Gratings

Because each single fringe reflects light with different phase shifts, interference occurs and most of the light is being erased. But the reflections with equal phase shift accumulate to a strong reflection peak. The reflection of the whole grating is the sum of all these thousands of very small single reflections. Fig. 3 explains this behavior in more detail. Top of Fig. 3 shows a fiber with a 10-fringe Bragg grating. Light enters from the left side. Below there are three light beams with different wavelengths. The upper one has precisely the wavelength of the grating period and all single fringe reflections are reflected in phase and therefore add up to an energy level of 10 times a single grid reflection. The next light beam below has a 10% higher frequency so that 11 light periods have the length of the 10 grid periods. All single reflections therefore have different phases, they interfere and compensate each other to zero resulting in a pole of the reflection function. The same happens with the lowest light beam which has a 10% lower frequency so that 9 light periods have the length of 10 grid periods.

What happens when the entering light differs from the grid count by ± 1.5 ? Then the phase vectors turn ± 1.5 times ($\pm 540^\circ$) over the total length of the grating. The first vectors in the 360° turn interfere to zero and the vectors of the remaining half turn accumulate, but the sum must be multiplied by $2/\pi$ because the reflected light vectors of these fringes differ in phase from 0° to 180° . Therefore the amplitude of the first side lobe is $2/(3*\pi)$, for the next side lobe $2/(5*\pi)$ and so on. The function of the reflection is a $\sin(x)/x$ -function.

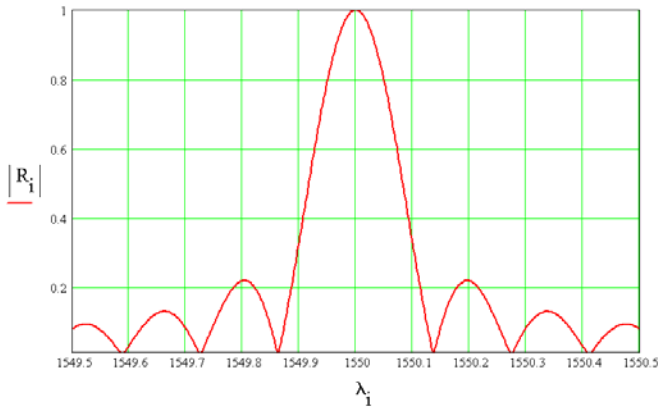


Fig. 4: Calculated normalized reflection of low reflecting Bragg gratings (<20% reflection) of 6 mm length and $\lambda = 1550$ nm wavelength

Fig. 4 shows the calculated spectral reflection of a 6-mm grating with 1550 nm peak wavelength.

This simple theory complies quite well with low reflective Bragg gratings (<20% peak reflection factor) while the theory of high reflective Bragg gratings (>90% peak reflection factor) is much more difficult and not a subject of this paper. However, a commentary about these two different kinds of FBG follows in chapter 4. The calculation of the spectral function of low reflective Bragg gratings will be explained next:

The specified wavelength of a FBG is the wavelength in vacuum. Inside a fiber the wavelength is shorter (divided by the refraction index of glass). Because the reflected light travels forth and back, reflected light beams of the single grids are in phase if an integer of light wavelength fits into two times the grid distance.

The grid spacing G_s therefore calculates:

$$G_s = \frac{\lambda_0}{2 * n} \quad (1)$$

Peak wavelength is λ_0 , n is the refraction index of the fiber. ($n=1.46$, typical for FBG and $\lambda_0 = 1550$ nm $\rightarrow G_s = 530$ nm).

Vice versa by altering the grid spacing G_s the wavelength of the reflected peak can be changed.

With a given length of the grating, e.g. $G_l = 6$ mm, the fringe count N can be calculated as:

$$N = \frac{G_l}{G_s} \quad (2)$$

Equation (1) inserted into equation (2) gives:

$$N = \frac{2 * n * G_l}{\lambda_0} \quad (3)$$

The result is $N = 11300$ grids ($\lambda_0 = 1550$ nm, $G_l = 6$ mm). Because light frequencies with wave counts of $N \pm 1$ per grating length interfere to zero, the pole distance Pd of the wavelength spectrum calculates:

$$Pd = \frac{\lambda_0}{N} \rightarrow Pd = 137 \text{ pm} \quad (4)$$

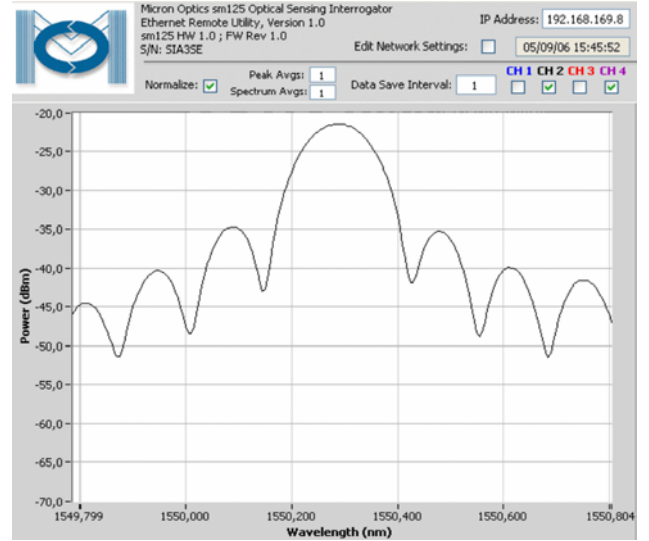


Fig. 5: A 6-mm Bragg grating (15% reflection) measured with interrogator sm125 from Micron Optics

Equation (3) inserted into equation (4) gives:

$$Pd = \frac{(\lambda_0)^2}{2 * n * G_l} \quad (5)$$

The result is a pole distance $Pd = 137$ pm. The main peak has twice the width (274 pm) from pole to pole. The whole function of the reflected spectrum R_i can be calculated according to equation (6).

$$R_i = \frac{\lambda_0}{\pi * N * \Delta \lambda_i} * \sin\left(\frac{\pi * N * \Delta \lambda_i}{\lambda_0}\right) \quad (6)$$

The wavelength λ_i of the x-axis is $\lambda_i = \lambda_0 + \Delta \lambda_i$. $\Delta \lambda_i$ runs over a range of 1000 pm in Fig. 4, Fig. 5 and Fig. 6.

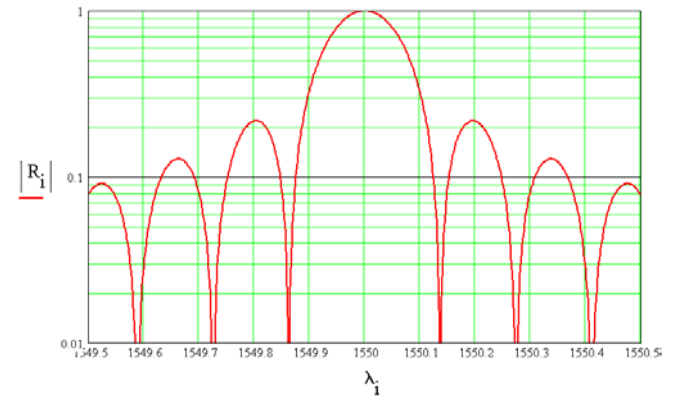


Fig. 6: Same function as in Fig. 4, only y-axis is logarithmic

Normally the width of the reflection peak is not defined by the pole-to-pole distance but by the definition of *FWHM* (Full-Width-Half-Maximum) that is the width at 50% of the main peak level. The function $\sin(x)/x$ is equal to 0.5 for $x = 1.8955$. The *FWHM* can then be calculated according to equation (7).

$$FWHM = 2 * \frac{1.8955 * \lambda_0}{\pi * N} \quad (7)$$

$$FWHM = 1,2067 * Pd$$

Equation (3) inserted into equation (7) gives:

$$FWHM = \frac{1.8955 * \lambda_0^2}{\pi * n * GL} \quad (8)$$

n = refraction index (1.46); GL = grating length (6 mm);
 $\lambda_0 = 1550 \text{ nm} \rightarrow FWHM = 165 \text{ pm}$

Fig. 5 shows a real measured spectrum of a 6-mm FBG. An interrogator sm125 from Micron Optics Inc. was used. Fig. 6 is the calculated spectrum. Both measured spectrum and calculated spectrum show almost identical characteristics. Only the deep poles in the calculated plot are different. The reason for this is that the interrogator obviously cannot follow the very fast signal slopes of the poles.

4. Two Different Methods to Induce Fiber Optic Bragg Gratings

Excimer laser with wavelengths of about 240...250 nm are used to induce the Bragg gratings. The interference pattern can be generated with the help of a phase mask (see Fig. 7) or by splitting laser beams (see Fig. 8). The standard procedure to make high reflective FBGS (>90% peak reflectivity) is to dismantle a standard telecom fiber (remove the acrylate or polyimide coating), expose the fiber to the ultraviolet interference pattern and then embed it again in a suited coating.

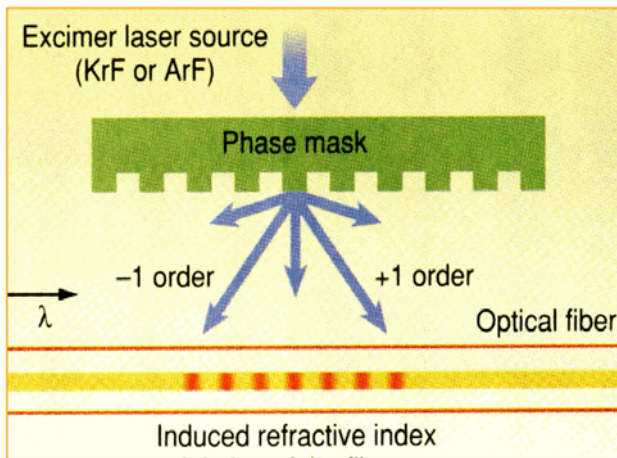


Fig. 7: Bragg grating induced by a laser and a phase mask

If the FBGS are to measure strain, polyimide coating is the right choice because acrylate is too soft and cannot precisely transfer the strain from the specimen to the fiber; especially not at high temperatures. The energy of the exposure is in the range of several hundred J/cm² causing a 0.01% ...0.1% change of the refractive index. While standard communication fibers may be strained up to 60,000 $\mu\text{m}/\text{m}$ the high reflective Bragg fibers break very often already at much lower strains. This is caused by the dismantling procedure which must be done very carefully. To avoid this problem a second method was developed to produce FBGS.

The inscription of the Bragg gratings is done on the fly during the fiber pulling process (see Fig. 8) and after that the fiber is being embedded into the coating. No subsequent dismantling process is then required.

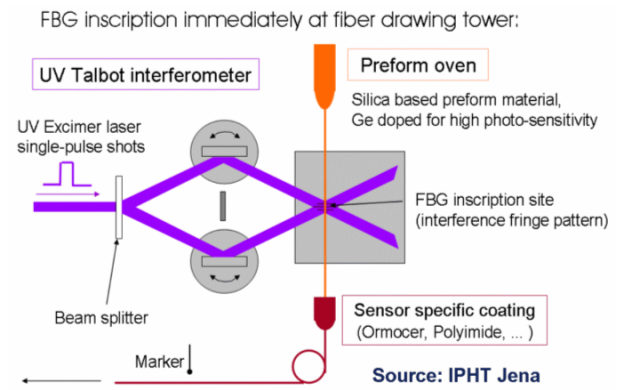


Fig. 8: FBG gratings produced on the fly

The preferred coating material of this process is ORMOCER (organic modulated ceramic) because its Young's modulus is comparatively high. Such sensors can be obtained from FBGS Technology GmbH Jena. Because the exposure is done on the fly only one single inscription UV-laser flash is triggered for each Bragg grating. The flash time has to be very short (nano-second range) to get precise gratings. Therefore the total energy of the exposure is only approximately 1/1000 of the high reflective FBGS's in the range of several hundred mJ/cm². However, since the photo sensitivity of the fiber core is very high at low energy levels, a reflectivity of 10%....20% can still be achieved.

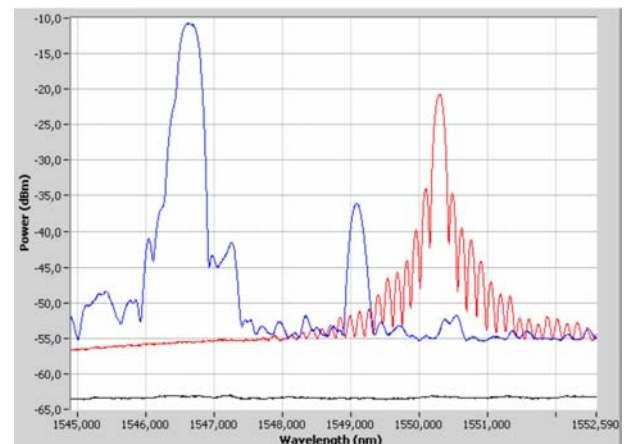


Fig. 9: Reflection peaks of a high reflective (left) and a low reflective (right) Fiber Optic Bragg Sensor

Fig. 9 shows typical reflection peaks of low and high reflective FBGS. The spectrum of the low reflective FBG (20%) on the right side looks pretty much like the theoretical function, and the peak width (FWHM) is small. On the left side of Fig. 9 the response of a high reflective (>90%) FBG show a much broader peak and almost no side lobes. The side lobes can be suppressed by apodizing, that means the energy of the inscription process is modulated in form of a Gaussian distribution over the length of the grating.

High reflective FBG sometimes also show unwanted smaller disturbance peaks like the small one in the middle of Fig 9 which is generated by the same grating as the left main peak.

5. Temperature and Strain Sensitivity

The wavelength of a FBGS changes with strain and temperature according to equation (9)

$$\frac{\Delta\lambda}{\lambda_0} = k * \varepsilon + \alpha_\delta * \Delta T \quad (9)$$

$\Delta\lambda$ = wavelength shift

λ_0 = base wavelength at test start

$$k = 1-p \quad (10)$$

p = photo-elastic coefficient, $p = 0.22$

k = gage factor, $k = 0.78$

ε = strain

ΔT = temperature change in K

α_δ = change of the refraction index,

$\alpha_\delta = 5 \dots 8 * 10^{-6}/K$

$$\alpha_\delta = \frac{\delta n / n}{\delta T} \quad (11)$$

The first expression ($k * \varepsilon$) of equation (9) describes the strain impact caused by force (ε_m) and temperature (ε_T). The second part ($\alpha_\delta * \Delta T$) describes the change of the glass refraction index n caused only by temperature.

$$\varepsilon = \varepsilon_m + \varepsilon_T \quad (12)$$

ε_m = mechanically caused strain

ε_T = temperature caused strain

$$\varepsilon_T = \alpha_{sp} * \Delta T \quad (13)$$

α_{sp} = expansion coefficient per K of the specimen

Equations (10) to (13) inserted into equation (9) lead to equations (14) and (15) which describe the behavior of a FBGS under the impact of both strain and temperature.

$$\frac{\Delta\lambda}{\lambda_0} = (1-p) * (\varepsilon_m + \alpha_{sp} * \Delta T) + \frac{\delta n / n}{\delta T} * \Delta T \quad (14)$$

$$\frac{\Delta\lambda}{\lambda_0} = k * (\varepsilon_m + \alpha_{sp} * \Delta T) + \alpha_\delta * \Delta T \quad (15)$$

$$\alpha_{sp} \text{ of steel} = 11 \dots 13 * 10^{-6}/K$$

$$\alpha_{sp} \text{ of aluminum} = 22 \dots 23 * 10^{-6}/K$$

$$\alpha_\delta \text{ of refraction} = 5 \dots 8 * 10^{-6}/K$$

In case of a pure temperature sensor a Bragg grating is not stressed (the fiber then is fixed only at one point, sufficiently apart from the Bragg grating). The FBGS $\Delta\lambda/\lambda_0$ signal then changes only with temperature according to equation (16). In this case α is the thermal expansion coefficient α_{glass} of the fiber.

$$\frac{\Delta\lambda}{\lambda_0} = (1-p) * \alpha_{glass} * \Delta T + \frac{\delta n / n}{\delta T} * \Delta T \quad (16)$$

$$\text{or} \quad \frac{\Delta\lambda}{\lambda_0} = (k * \alpha_{glass} + \alpha_\delta) * \Delta T \quad (17)$$

$$\Delta T = \frac{1}{k * \alpha_{glass} + \alpha_\delta} * \frac{\Delta\lambda}{\lambda_0} \quad (18)$$

Equation for a temperature-measuring FBGS

$$\alpha_{glass} = 0.55 * 10^{-6} / K$$

The expansion coefficient α_{glass} of the fiber is very low; almost zero. The biggest impact results from the temperature dependent change of the refraction index α_δ . When a fiber is fixed to a specimen, the FBGS signal $\Delta\lambda/\lambda_0$ changes with the strain ($\varepsilon_m + \varepsilon_T$) of the specimen and therefore the thermal expansion coefficient is α_{sp} then and not α_{glass} .

$$\frac{\Delta\lambda}{\lambda_0} = k * \varepsilon_m + (k * \alpha_{sp} + \alpha_\delta) * \Delta T \quad (19)$$

$$\varepsilon_m = \frac{1}{k} * \frac{\Delta\lambda}{\lambda_0} - (\alpha_{sp} + \frac{\alpha_\delta}{k}) * \Delta T \quad (20)$$

Equation for a strain-measuring FBGS

When the FBGS is fixed to the specimen on a region without mechanical strain ($\varepsilon_m=0$) it works as a temperature compensation FBGS. Its signal calculates according to equations (21) and (22).

$$\frac{\Delta\lambda}{\lambda_0} = (k * \alpha_{sp} + \alpha_\delta) * \Delta T \quad (21)$$

$$\Delta T = \frac{1}{k * \alpha_{sp} + \alpha_\delta} * \frac{\Delta\lambda}{\lambda_0} \quad (22)$$

Equation for a temperature compensation FBGS

6. Temperature Compensation

Because temperature has a very strong impact on the FBGS signals, precise strain measuring results can only be achieved with proper temperature compensation. Normally an additional temperature-measuring FBGS is used and the signal of the strain-measuring FBGS is corrected by calculation. There are two different methods possible. At first it is possible to measure the temperature with a pure temperature-measuring FBGS and secondly to measure the temperature impact using a temperature compensation FBGS. The more simple solution to compensate temperature impact is to use a compensation FBGS. A FBGS (mechanically identical to the active strain-measuring FBGS and may be also on the same fiber) has to be placed on a location of the specimen with zero mechanical strain ($\varepsilon_m = 0$). Correct results can be achieved for the mechanical strain ε_m according to equation (24) by subtracting the signal of the compensation FBGS from the signal of the active strain-measuring FBGS. Equation (23) = (19) – (21).

$$\frac{\Delta\lambda_m}{\lambda_{0m}} - \frac{\Delta\lambda_c}{\lambda_{0c}} = k * \varepsilon_m \quad (23)$$

$$\varepsilon_m = \frac{1}{k} * \left(\frac{\Delta\lambda_m}{\lambda_{0m}} - \frac{\Delta\lambda_c}{\lambda_{0c}} \right) \quad (24)$$

$\Delta\lambda_m$ = wavelength shift of strain-measuring FBGS

λ_{0m} = base wavelength of strain-measuring FBGS

$\Delta\lambda_c$ = wavelength shift of compensation FBGS

λ_{0c} = base wavelength of compensation FBGS

Measurements at very high temperatures (several hundred °C) must take into account that the base wavelengths of both FBGS change considerably with temperature and therefore λ_0 (the original wavelength at room temperature) has to be replaced in all equations above by

$$\lambda_{0T} = \lambda_0 + \Delta\lambda_T \quad (25)$$

$\Delta\lambda_T$ is the change of wavelength of FBGS_{comp} caused by temperature change.

But it is not always possible to find a position without strain on the specimen to fix a compensation FBG. In these cases the method first mentioned – pure temperature measurement - has to be applied. When the temperature is captured by a temperature-measuring FBGS according to equations (16) to (18) the calculation of strain becomes a little more complex. Replacing ΔT in equation (20) by the term for ΔT in equation (18) leads to equation (26).

$$\varepsilon_m = \frac{1}{k} * \left(\frac{\Delta\lambda_m}{\lambda_{0m}} - \frac{\Delta\lambda_T}{\Delta\lambda_{0T}} * \left(\frac{k * \alpha_{sp} + \alpha_\delta}{k * \alpha_{glass} + \alpha_\delta} \right) \right) \quad (26)$$

$\Delta\lambda_T$ = wavelength shift of temperature-measuring FBGS

λ_{0T} = base wavelength of temperature-measuring FBGS

Because $k * \alpha_{glass}$ is almost zero this term may be neglected or can be included in α_δ by increasing α_δ by $0.4 * 10^{-6}$. Equation (26) simplifies then to equation (27).

$$\varepsilon_m = \frac{1}{k} * \left(\frac{\Delta\lambda_m}{\lambda_{0m}} - \frac{\Delta\lambda_T}{\Delta\lambda_{0T}} * \left(\frac{k * \alpha_{sp}}{\alpha_\delta} + 1 \right) \right) \quad (27)$$

If equation (26) or (27) is used, it is necessary to know the expansion coefficient α_{sp} of the specimen and the index of refraction α_δ very precisely. (The index of refraction depends especially strong on the amount of Germanium dotting of the fiber.)

7. FBGS Interrogators

When FBGS are being strained the wavelength of the reflection peaks will be shifted. For measuring strain with FBGS it is necessary to measure these shifts very precisely. Resolution and short-term stability of ± 1 pm is required, if strain values of $1 \mu\text{m/m}$ are to be measured.

1 pm resolution of peak wavelength of 1550 nm means a relationship of $>10^6$. There exist many different principles to analyze such optical spectrums. For laboratory tasks, interferometers are often used. But they are not so well suited to robust industrial applications. In industrial environments other principles dominate. Three of them will be briefly explained below:

The edge filter principle uses special optical filters with wavelength-dependent transparencies. In a differential configuration (as shown in Fig. 10) the reflected light of a

FBG is split into two equal beams and then fed through two different edge filters with opposite characteristics. The transparency of "Filter a" increases with wavelength while the transparency of "Filter b" decreases. A differential photo-diode behind the filters a and b generates an electrical signal proportional to the difference of light behind the two filters.

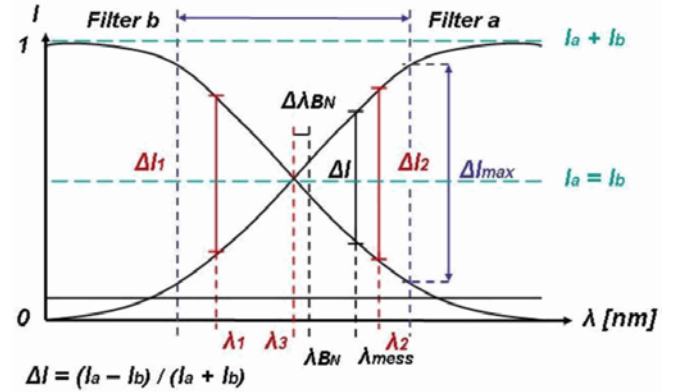


Fig. 10: Edge filter interrogator

A shift of the FBG wavelength therefore changes the amplitude of the output signal of the differential diodes. This principle is able to provide high bandwidth at low price. But only one FBGS signal can be measured with an edge filter channel at a time. This principle enables only the value of the peak wavelength to be output but cannot provide information about a spectrum. Because it is an analog (level-depending) principle its accuracy and stability is low and higher levels of scattered light can corrupt the results completely.

For FBGS with wavelengths in the range of 800 nm, CCD based interrogators are well suited. A holographic grating reflects different wavelengths to different pixels of the CCD-line. With interpolation algorithms the resolution of the CCD can be increased by two orders of ten providing a

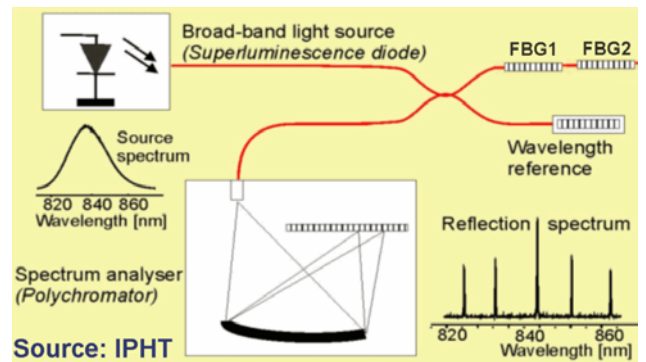


Fig. 11: CCD based interrogator for 800 nm band

total resolution of 1 pm. The CCD principle can be made pretty fast (>1000 M/s) and provides good accuracy and a good signal-to-noise ratio. It captures the whole spectrum and therefore can measure many FBGS signals with different wavelengths simultaneously. Normally this principle is used in the 800-nm band because affordable CCDs are based on silicon technology and therefore work only in the near infrared light-band.

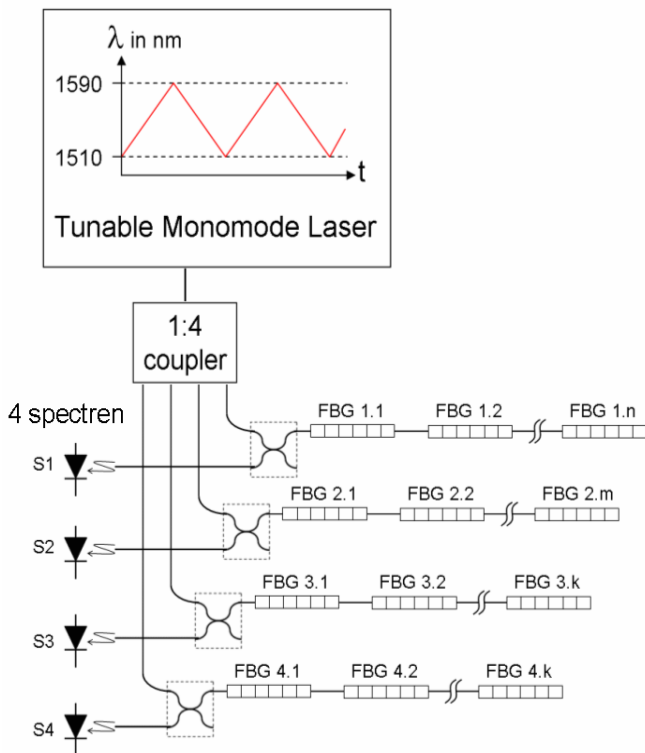


Fig. 12: High resolution interrogator with tunable laser

For the C-band (~1550 nm), interrogators with tunable lasers represent the top-class instruments [4]. Other interrogator principles use broad-band light sources and therefore only a very small part of the light energy is related to the small bandwidth of a FBG. Therefore the reflected peak energy is very low. A tunable laser concentrates all its energy in an extremely small bandwidth and by sweeping over the whole bandwidth range (see Fig. 12) it scans the spectrum with high power and can provide an excellent signal-to-noise ratio.

Because of this high signal-to-noise ratio, FBGS with reflectivities down to <1% can still be measured with high precision. Because of the high energy budget the tuned laser output signal can be split into many output channels without losses in signal quality. Fig. 12 shows 4 channels with connected fibers. Each channel can measure many Bragg sensors positioned on its fiber (e.g. FBG1.1FBG1.n on the first channel). Because one receiver per channel exists it is also possible to capture a full spectrum per channel. This is a big advantage because the available bandwidth then is four times 80 nm = 320 nm. So FBGS with equal wavelengths can be measured if they are on different channels and the total number of connectable FBGS is four times higher in comparison to interrogator principles which work with only one receiving and signal conditioning unit.

8. Measuring System for Fiber Bragg Grating Sensors and Strain Gages

In experimental stress analysis tests, strain-measuring systems are the fundamental tool used very frequently. In addition to the matured foil strain gage technology - invented 70 years ago - the new technology of Fiber Bragg Grating Sensors (FBGS) - now 12 years old - is the second important principle for strain acquisition. Actually this is a relatively young method and it is far from maturity, however

it provides many advantages in special applications as pointed out in chapter 2. The fiber and the Bragg grating technology can be controlled pretty well today and represent no problem any more. The main problem comes from the requirement to induce the strain precisely into the fiber.



Fig. 13: SI-405 optical interrogator together with MGCplus

Embedding and gluing procedures of the fibers, temperature correction, prevention of humidity dependency and all these issues very well known from foil strain gage technology are also topics of FBGS.

The analogy with equal strain gage subjects is obvious and the applied methods often have to be the same. In R&D analysis and also for validation tests of FBGS, strain gages often are used in addition to FBGS to assure the results. For such test environments, systems which are able to connect and measure FBGS and strain gages simultaneously and enable post processing for both provide big advantages.

Fig. 13 shows such a system containing an optical interrogator SI-405 to measure the FBGS signals and an MGCplus to measure strain gages (and if necessary a lot of other sensors like PT100, thermocouples, voltage and current sources etc.). The PC that is required in addition is not shown in Fig. 13.

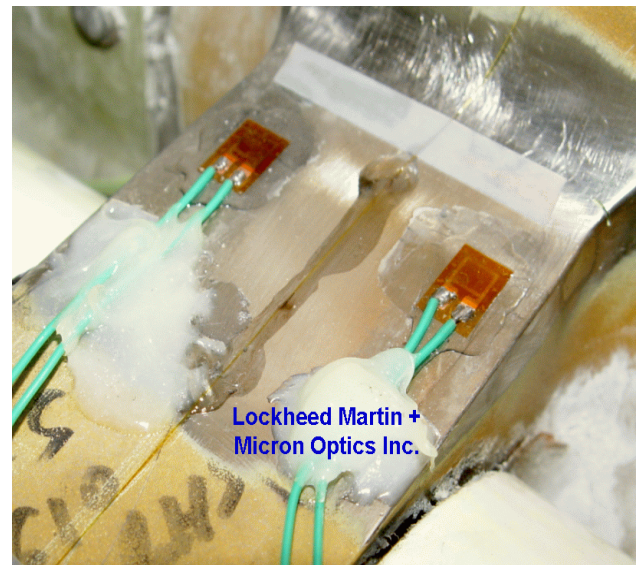


Fig. 14: Application of two strain gages and one FBG sensor

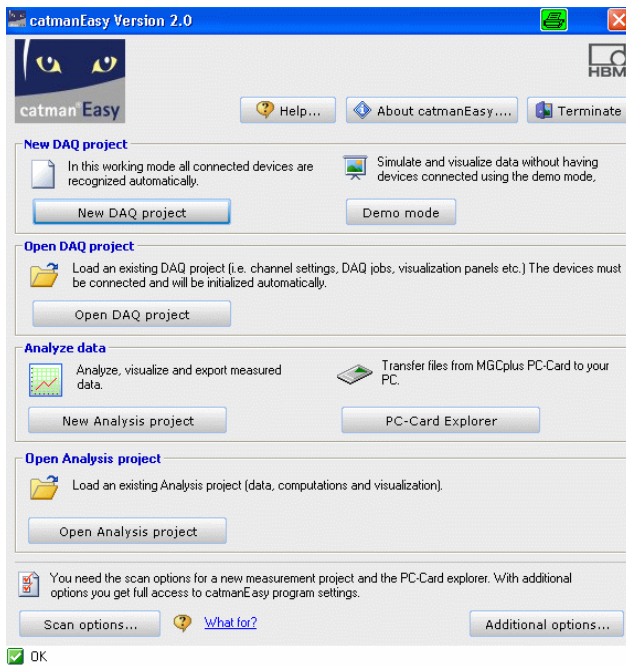


Fig. 15: Start panel of catmanEasy©

CatmanEasy© is the software used for data acquisition, online graphic and post processing. Fig. 15 shows the start panel of catmanEasy©. If the “New DAQ project” button is pressed the connected instruments are automatically scanned and all their measuring channels activated and displayed in a channel list. Fig. 16 is an example for such a channel list. The access to various online graphs (example is shown in Fig. 17) is also provided by this panel (not shown in Fig. 16). Channels to be displayed in a chosen online graph can easily be copied out of the channel list by drag and drop and put into the diagrams.

		Name	Connection
1		MICRON_NTP_TIME	micronOptics_sm125 CH 1
2		Fiber_A23_Sensor_1	micronOptics_sm125 CH 1-1
3		Fiber_B5_Sensor_1	micronOptics_sm125 CH 2-1
4		Fiber_B5_Sensor_2	micronOptics_sm125 CH 2-2
5		Fiber_B5_Sensor_3	micronOptics_sm125 CH 2-3
6		Fiber_B5_Sensor_4	micronOptics_sm125 CH 2-4
7		Fiber_B5_Sensor_5	micronOptics_sm125 CH 2-5
8		Demo_Fiber_Sensor_1	micronOptics_sm125 CH 3-1
9		Time DEVICE_2 (Sample rate 1)	Time
10		S/G 300	HBM_MGCplus CH 1
11		S/G 301	HBM_MGCplus CH 2
12		S/G 302	HBM_MGCplus CH 3
13		Temperature	HBM_MGCplus CH 4
14		Channel 14	NC
15		Channel 15	NC

Fig. 16: Channel list with FBG sensors and strain gages

All measured data is automatically buffered and can be stored after completion of the test under individual names or can be stored periodically e.g. every 10 minutes to avoid power down data losses.

For post processing purposes these data files can be accessed by “Open DAQ projects” button on the start panel (Fig. 15).

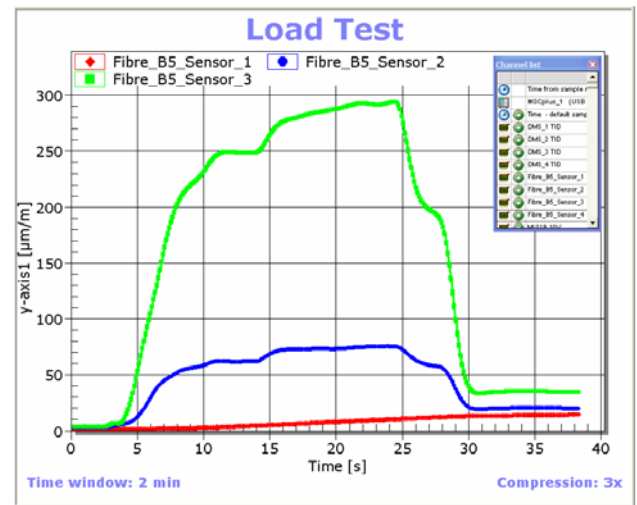


Fig. 17: Online graphic of a load test

The “Test Explorer” panel opens (Fig. 19) then and stored data files can be selected and easily activated by drag and drop too. Under “Computations” computed channels can be generated (left side of Test Explorer). To do this, formulas can be set up which include measured channel data and all mathematic functions shown in Fig. 19. By the “Paste” button a large variety of higher mathematical functions will be offered additionally. Functions in other panels provide FFT spectrums, filter algorithms and last but not least, all necessary functions for stress analysis like rosette calculation (Fig. 18).

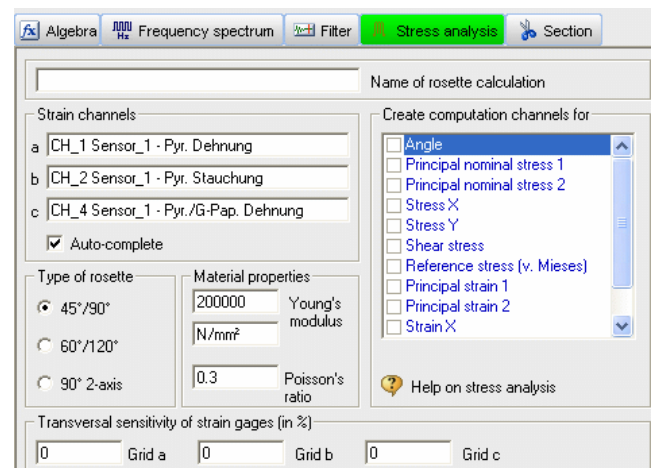


Fig. 18: Computing functions for rosette calculations

In parallel to all the data acquisition, real time displays and post processing calculations of physical quantities, catmanEasy© can also display and store the four spectrums measured by the interrogator SI-401 (Fig. 20). The buffered data can be saved manually by pressing the “Save now” button or automatically every “n” minutes by activating “Save automatically every “n” minutes”.

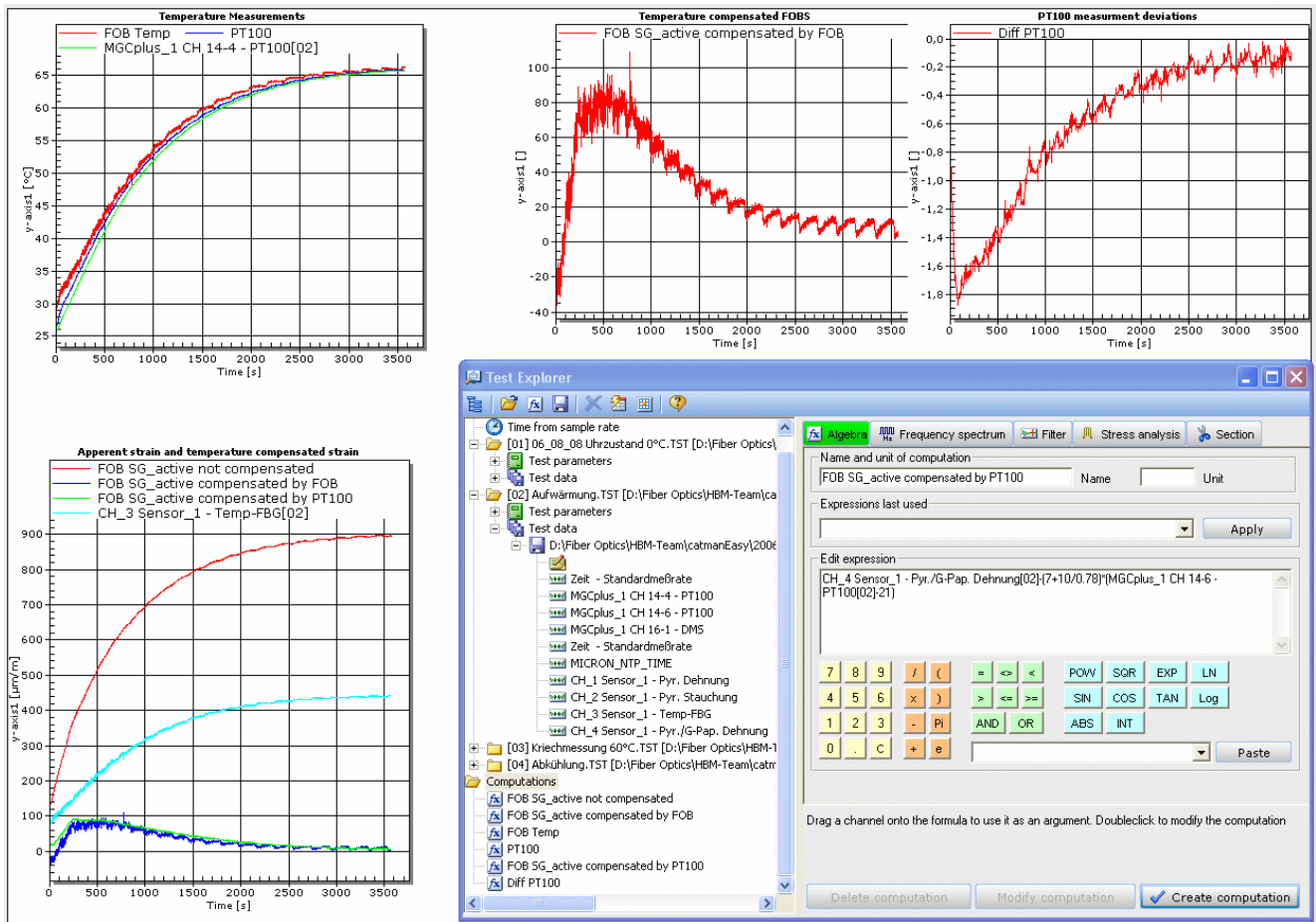


Fig. 19: Test Explorer (setup for post processing and some diagrams with post-processed data)

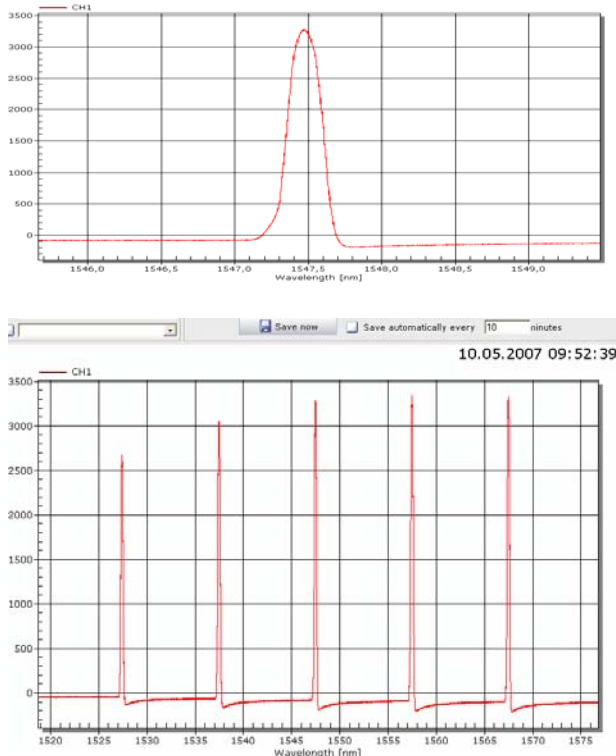


Fig. 20: Wavelength spectrum

9. References

- [1] Mitschke, F.: Glasfasern, Physik und Technologie; ELSEVIER SPEKTRUM Akademischer Verlag, ISBN 3-8274-1629-9
- [2] Trutzel, M.: Dehnungsermittlung mit faseroptischen Bragg-Gitter-Sensoren, Berlin 2001, D83; Dissertation
- [3] Dyer S. D., Williams P. A., Espejo R. J., Kofler J.D., Etzel S. M.: Fundamental limits in fibre Bragg grating Peak wavelength measurements; National Institute of Standards and Technology, Optoelectronics Division, Boulder, CO 80305 USA 17th International Conference on Optical Fibre Sensors Proceedings of SPIE Vol. 5855
- [4] Zhou Z., Graver T. W., Hsu L., Ou J.: Techniques of Advanced FBG sensors: fabrication, demodulation, encapsulation and the structural health monitoring of bridges; Pacific Science Review, vol. 5, 2003, pp. 116-121
- [5] Schroeder., Ecke , Apitz , Lembke, Lenschow: A fibre Bragg grating sensor system monitors operational load in a wind turbine rotor blade; ©2006 IOP Publishing Ltd., Meas. Sci. Technology 17 (2006) 1167-1172